

SimFlow: Simplified and End-to-End Training of Latent Normalizing Flows

Qinyu Zhao^{1,2}, Guangting Zheng², Tao Yang², Rui Zhu^{2†}, Xingjian Leng¹,
Stephen Gould¹, Liang Zheng¹

¹Australian National University, ²ByteDance Seed

[†]Project lead

Abstract

Normalizing Flows (NFs) learn invertible mappings between the data and a Gaussian distribution. Prior works usually suffer from two limitations. First, they add random noise to training samples or VAE latents as data augmentation, introducing complex pipelines including extra noising and denoising steps. Second, they use a pretrained and frozen VAE encoder, resulting in suboptimal reconstruction and generation quality. In this paper, we find that the two issues can be solved in a very simple way: just fixing the variance (which would otherwise be predicted by the VAE encoder) to a constant (*e.g.*, 0.5). On the one hand, this method allows the encoder to output a broader distribution of tokens and the decoder to learn to reconstruct clean images from the augmented token distribution, avoiding additional noise or denoising design. On the other hand, fixed variance simplifies the VAE evidence lower bound, making it stable to train an NF with a VAE jointly. On the ImageNet 256×256 generation task, our model SimFlow obtains a gFID score of 2.15, outperforming the state-of-the-art method STARFlow (gFID 2.40). Moreover, SimFlow can be seamlessly integrated with the end-to-end representation alignment (REPA-E) method and achieves an improved gFID of 1.91, setting a new state of the art among NFs.

Date: December 4, 2025

Contact: qinyu.zhao@anu.edu.au

Project Page: <https://qinyu-allen-zhao.github.io/SimFlow/>

1 Introduction

Normalizing flows (NFs) [9, 17, 18, 29, 49, 70, 72] model a data distribution by transforming a prior distribution (*e.g.*, the normal distribution) via invertible mappings. For easier training and better generation, state-of-the-art methods [17, 18] adopt two strategies: 1) using a variational autoencoder (VAE) [50] to train a latent NF, and 2) adding noise to VAE latents during NF training as data augmentation.

However, there are two limitations with the above strategies. First, while adding random noise smooths latent space for more generalizable NF modeling, it complicates the pipelines. Specifically, NFs trained with noisy inputs generate noisy outputs, so existing works have to introduce an additional denoising process, such as score-based denoising [70], a fine-tuned VAE decoder [17], or a flow matching model for denoising [18]. The extra noising and denoising steps complicate the training and inference processes.

Second and more importantly, these methods use a frozen VAE encoder, which leads to suboptimal recon-

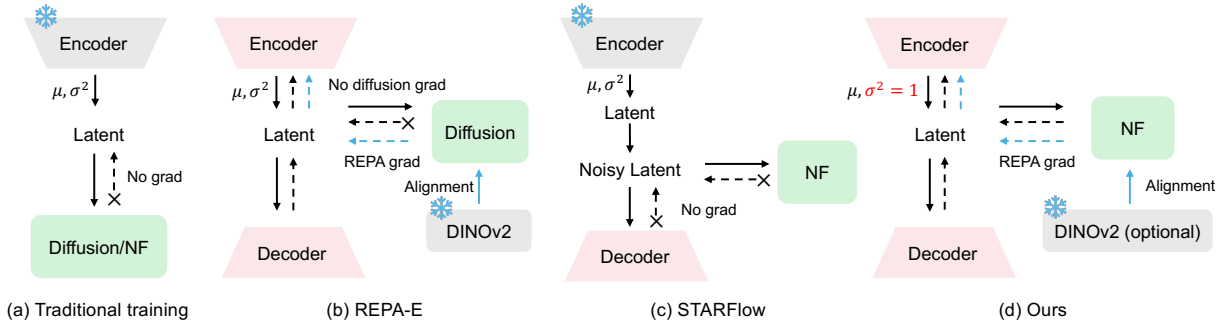


Figure 1 Comparison of our framework with closely-related methods. (a) Standard practice trains a VAE first and then train a generative model with the VAE frozen. Note that, for each image, the VAE encoder outputs the mean μ and the variance σ^2 of a Gaussian, from which a set of tokens is sampled. The variance σ^2 is usually very small in a standard pretrained VAE. (b) REPA-E [33] jointly trains diffusion with VAE using the REPA loss [69], and the diffusion gradient is stopped before the VAE to avoid latent collapse (where the token variation decreases and the generation quality degrades). (c) STARFlow [17] trains NF and decoder on noisy latent with the encoder frozen. (d) We train an NF and a VAE in an end-to-end way from scratch. There is no stop-gradient operator, significantly simplifying prior frameworks. Solid arrows indicate the forward pass, while dashed arrows denote gradient flows. We label frozen modules in gray, generative models in green, and VAE modules involved in training in red.

struction and generation quality. For *reconstruction*, the encoder is sensitive to noise because it is not trained under noise augmentation introduced for NFs. Possibly, if images are very close to each other in the latent space, noise perturbations may severely degrade the latents. While it is feasible to fine-tune the decoder [17], reconstruction quality remains poor, because some encoded information is already lost due to noise (for results see Section 5.2). For *generation*, now that the encoder is not optimized jointly with an NF, the latent space may not be best suitable for NF modeling.

In this paper, we solve both issues at the same time by introducing SimFlow, a simple end-to-end training framework for latent NFs. Our key idea is to fix the encoder-predicted variance to a constant (for instance, 0.5). On the one hand, this method has similar effects with adding noise to latents [17], that is, to smooth the latent space and improve generalization, but greatly simplifies the pipeline. Note that pretrained VAEs tend to predict extremely small variance (*e.g.*, less than 0.01), which collapses a token distribution to nearly a single point. In contrast, our method of fixing variance to a larger value ensures each latent token is sampled from a broader distribution rather than a nearly deterministic result. Meanwhile, the decoder learns how to reconstruct clean images from the augmented token distributions during VAE training. In this way, our approach removes the need for additional noising or denoising design.

On the other hand, fixing the variance to a value like 0.5 enables effective end-to-end training of latent NFs, making the VAE latents compatible with NF modeling. From the VAE evidence lower bound (ELBO) perspective, this method makes the entropy term become a constant, which simplifies the training objective to consist of only the reconstruction loss and the generation loss. We find that it is much easier to balance between reconstruction and generation than to

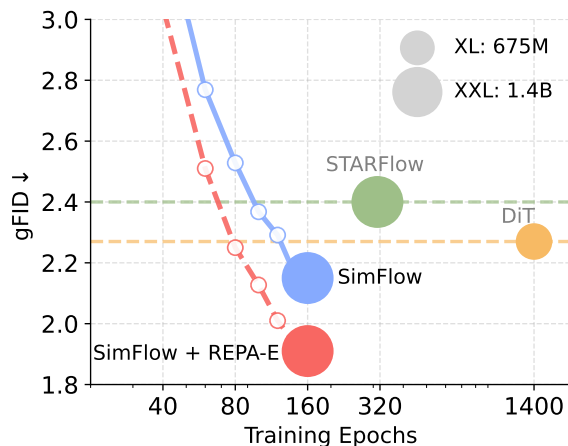


Figure 2 Comparing SimFlow with prior works. On ImageNet 256×256 , our end-to-end trained model SimFlow achieves significantly better generation quality than the state-of-the-art NF model STARFlow [17] with much fewer training epochs. Training SimFlow with REPA-E [33] further improves gFID.

train the whole framework. A comparison of SimFlow with prior works is shown in Figure 1.

On the ImageNet 256×256 generation benchmark, SimFlow achieves a gFID score of 2.15, surpassing the prior work STARFlow (gFID 2.40) [17], as shown in Figure 2. This is also the first report that NFs outperform DiT [45], a representative diffusion model. While SimFlow has a larger model size, its convergence rate is more than 8 times faster than DiT. Importantly, our framework is fully compatible with REPA-E [33]: aligning NF features with DINOv2 [3] and training both the VAE and NF using the alignment loss. Combining SimFlow with REPA-E further decreases gFID to 1.91 on Image 256×256 and achieves a gFID score of 2.74 on ImageNet 512×512 , establishing new state-of-the-art performance among NF-based models.

2 Related work

Normalizing flows (NFs) [8–11, 13, 29, 31, 38, 39, 43, 49, 62, 72] are a useful framework for density estimation, visual generation, and text generation. In this paper, we mainly adopt autoregressive flows (AFs) [17, 70]. In each invertible transformation of an AF, each token is transformed conditioned on previous tokens. Representative AFs include IAF [30], MAF [42], neural AF [23], and T-NAF [44]. More recently, TARFlow [70] leverages causal Transformers and simplifies the log-determinant term in the loss function, leading to notable improvements in generation quality. STARFlow [17] extends TARFlow into the VAE latent space and further improves the NF performance.

VAEs with fixed variance or noise-augmented training. Sun et al. [57] introduce σ -VAE, which has a fixed variance, and later works adopted this technique [27, 58]. Other studies [40, 46, 66] introduce noise or perturbation in the latent space. While these approaches are similar to ours, they are motivated differently and do not explore joint training with generative models. In Section 4.3, we show that our perspective provides a unified explanation of why these methods actually allow for stable end-to-end training.

Joint training of generative models with VAEs. The standard practice is to train a VAE on the reconstruction task first and then train a generative model with the VAE frozen [1, 15–17, 35, 37, 41, 45, 47, 48, 53, 56]. But an important question is whether the pretrained VAE space is suitable for training a generative model. Without solving this, a possible consequence is that a VAE with excellent reconstruction ability leads to poor generation quality of the generative models trained on the latent space [32, 67].

End-to-end training of generative models with VAEs is appealing because it not only streamlines the training pipeline but is also expected to make the VAE latent space more suitable for generation. Early exploration [49, 55, 61] is not stable in training and does not achieve competitive performance on a large-scale dataset like ImageNet 256×256 . Recently, REPA-E [33] reported an FID of 1.12 on ImageNet 256×256 with end-to-end training. In REPA-E, the gradient of the REPA loss [69] flows through the diffusion model to the VAE, while the gradient from the diffusion model does not flow to the VAE (see Figure 1(b)). When the latter is allowed, they observe latent space collapse, where the latent variance shrinks quickly, and the generation quality is poor. Different from REPA-E, SimFlow jointly trains NFs and VAEs from scratch without stopping any gradient, further simplifying the training framework.

3 Preliminaries

A standard VAE [28] consist of an encoder q_ψ and a decoder p_ω . Given an image \mathbf{i} , the encoder predicts mean $\boldsymbol{\mu}$ and variance $\boldsymbol{\sigma}^2$ of a Gaussian distribution $\mathcal{N}(\boldsymbol{\mu}, \text{diag}(\boldsymbol{\sigma}^2))$. A latent variable \mathbf{x} (a set of tokens) is sampled from $\mathcal{N}(\boldsymbol{\mu}, \text{diag}(\boldsymbol{\sigma}^2))$. The decoder is trained to reconstruct the image \mathbf{i} from \mathbf{x} . The VAE is trained with ELBO as follows:

$$\log p(\mathbf{i}) \geq \mathbb{E}_{\mathbf{x} \sim q_\psi(\mathbf{x}|\mathbf{i})} \left[\underbrace{\log p_\omega(\mathbf{i} | \mathbf{x})}_{\text{Reconstruction}} + \underbrace{\log p(\mathbf{x})}_{\text{Prior}} - \underbrace{\log q_\psi(\mathbf{x} | \mathbf{i})}_{\text{Entropy}} \right], \quad (1)$$

where the prior term is usually chosen as the normal distribution $\mathcal{N}(\mathbf{0}, \mathbf{I})$, and the prior and entropy terms are combined into a Kullback-Leibler (KL) divergence term.

Latent NFs [8, 9, 17, 29, 49] map the VAE latent distribution into a simple one $\mathbf{z} \sim p_0(\mathbf{z})$ (the normal distribution), via learning an invertible function f_θ . During training, the forward pass maps the sampled latent \mathbf{x} to $\mathbf{z} = f_\theta(\mathbf{x})$, following the change of variable formula:

$$p_{\text{NF}}(\mathbf{x}; \theta) = p_0(\mathbf{z}) \left| \det \left(\frac{\partial \mathbf{z}}{\partial \mathbf{x}} \right) \right| = p_0(f_\theta(\mathbf{x})) \left| \det \left(\frac{\partial f_\theta(\mathbf{x})}{\partial \mathbf{x}} \right) \right|. \quad (2)$$

NFs are trained with maximum likelihood estimation:

$$\max_{\theta} \mathbb{E}_{\mathbf{x} \sim p_{\text{latent}}} \log p_{\text{NF}}(\mathbf{x}; \theta). \quad (3)$$

At inference, \mathbf{z} is sampled from the target distribution $\mathbf{z} \sim \mathcal{N}(\mathbf{0}, \mathbf{I})$, and an inverse process maps \mathbf{z} to $\mathbf{x} = f_\theta^{-1}(\mathbf{z})$, which is then decoded by the decoder to images. In this way, f_θ^{-1} with the VAE decoder is a generative model, which maps Gaussian noise to new image samples.

This study mainly builds on STARFlow [17], as it achieves competitive performance compared to other generative models on the large-scale ImageNet dataset. That said, our end-to-end training framework is expected to be applicable to other latent NF models as well.

4 Method

In Section 4.1, we present SimFlow, our joint training framework for latent NFs, from two different perspectives: noise augmentation in NF training and the VAE ELBO formulation. In Section 4.2, we adopt REPA-E to further improve SimFlow. In Section 4.3, latent space is analyzed to show the effects of end-to-end training. Section 4.4 revisits and improves the classifier-free guidance (CFG) for NFs.

4.1 SimFlow: End-to-end training of latent NFs

Let f_θ denote the NF model, and let q_ψ and p_ω denote the encoder and decoder of a VAE, respectively. We set variance outputted from the encoder as a constant $\bar{\sigma}^2$. The encoder only predicts mean $\boldsymbol{\mu}$ for each image \mathbf{i} , and the latent variable \mathbf{x} is sampled from the Gaussian $\mathcal{N}(\boldsymbol{\mu}, \bar{\sigma}^2 \mathbf{I})$. The NF is trained to convert \mathbf{x} to Gaussian samples $\mathbf{z} = f_\theta(\mathbf{x})$, and the decoder learns to reconstruct the images from \mathbf{x} .

Our system is trained with the combined VAE and NF objective (details are in Section A):

$$\max_{\theta, \psi, \omega} \mathbb{E}_{\mathbf{i} \sim p_{\text{data}}} \mathbb{E}_{\mathbf{x} \sim q_\psi(\mathbf{x}|\mathbf{i})} [\log p_\omega(\mathbf{i} | \mathbf{x}) + \log p_{\text{NF}}(\mathbf{x}; \theta)], \quad (4)$$

where the entropy term is a constant and thus omitted. Note that we do not tune the weights of loss terms in Eq. 4 and simply set them to 1.0. We also add perceptual loss and adversarial loss [14] for VAE training [50].

From the noise-augmented training perspective, the distribution outputted by the VAE encoder can be decomposed into $\boldsymbol{\mu}$ and a Gaussian noise, $\mathbf{x} = \boldsymbol{\mu} + \boldsymbol{\epsilon}$, $\boldsymbol{\epsilon} \sim \mathcal{N}(\mathbf{0}, \text{diag}(\boldsymbol{\sigma}^2))$. Ideally, the token distribution is already augmented by noise $\boldsymbol{\epsilon}$. However, for a well-pretrained VAE, we observe that $\boldsymbol{\sigma}^2$ is usually very small. There are two main reasons. First, the KL term could have maintained the variance as regularization but is usually assigned a very small weight (*e.g.*, 10^{-5}), making its effect negligible. Second, if $\boldsymbol{\sigma}^2$ is large, it is hard for the decoder to reconstruct the image from the highly varying latent. Thus, the encoder shrinks the variance, making it easier to decode. As a result, the latent still needs noise augmentation for NF training.

In this work, we manually set σ^2 from the encoder to a constant $\bar{\sigma}^2$ and the VAE encoder embeds images into $\mathbf{x} = \boldsymbol{\mu} + \boldsymbol{\epsilon}$, $\boldsymbol{\epsilon} \sim \mathcal{N}(\mathbf{0}, \bar{\sigma}^2 \mathbf{I})$. The resulting ‘VAE+NF’ framework naturally becomes noise-augmented training. NF learns the distribution while the decoder is trained to reconstruct the image. This avoids additional noising and denoising steps, simplifying the prior frameworks.

From the VAE ELBO perspective, a straightforward way for end-to-end training is to follow the ELBO:

$$\mathbb{E}_{\mathbf{x} \sim q_\psi(\mathbf{x}|\mathbf{i})} [\log p_\omega(\mathbf{i} | \mathbf{x}) + \log p_{\text{NF}}(\mathbf{x}; \theta) - \log q_\psi(\mathbf{x} | \mathbf{i})], \quad (5)$$

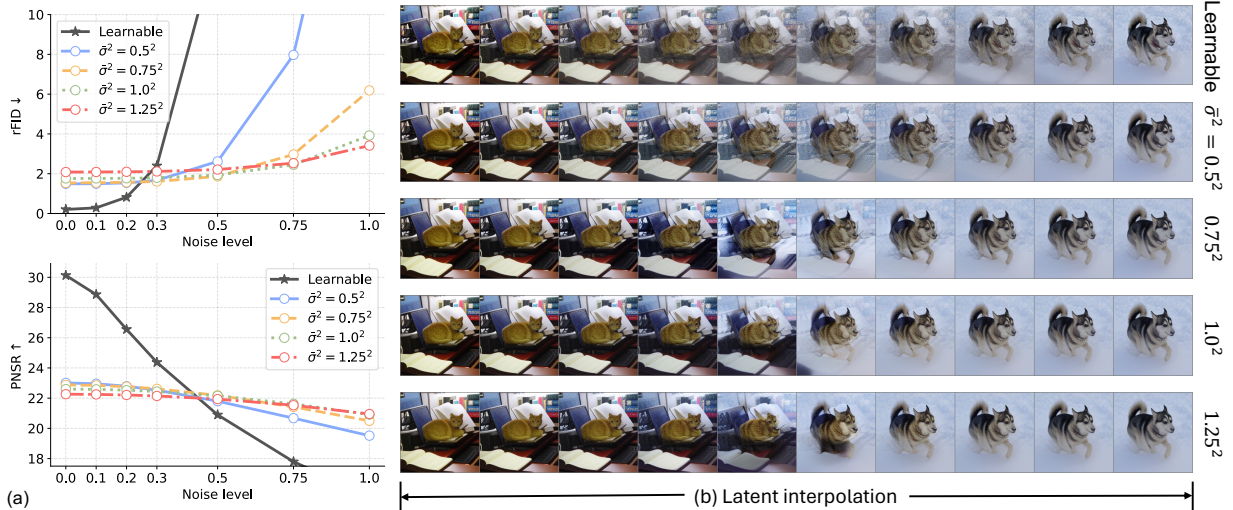


Figure 3 Robustness of VAEs with fixed variances. (a) A VAE with a large and fixed variance can maintain reconstruction quality under latent noise, while the performance of a VAE with learnable variance degrades significantly. (b) For VAEs with a large variance, the images reconstructed from linearly interpolated latents still clearly show the main subjects (the cat or the dog), rather than blending them. ‘Learnable’ indicates a standard VAE with learnable variance, while ‘ $\sigma^2 = x^2$ ’ denotes a VAE with a fixed variance of x^2 .

where the entropy term maintains variance not to be small, avoiding latent collapse [33, 61].

However, we empirically find it hard to balance the loss terms. The reconstruction term tends to reduce the variance, the NF term tends to shrink the predicted latent mean, while the entropy term tends to enlarge the variance. The tension makes the training sensitive to the loss weights and leads to suboptimal performance.

In SimFlow, because we manually set σ^2 as a constant, the entropy term becomes constant as well (see Section A.3). The objective now consists of only the reconstruction and generation terms. It then becomes easier to train the entire framework by simply assigning equal weights to both terms.

4.2 Representation alignment

Recent studies [33, 67, 69] show that alignment with features extracted from a representative model significantly benefits the training of a diffusion model. During training, REPA [69] extracts features with a pretrained representation model, such as DINOv2-B [3] and uses a projector to align the hidden states from a diffusion block with the DINO features. Besides, VAVAE [67] and REPA-E [33] report stronger benefits of alignment when training VAE or under joint training.

We adopt REPA to SimFlow to further improve the reconstruction and generation quality. As shown in Figure 1(d), we extract features from DINOv2-B and use a projector to align the hidden states of NF with DINO features. Note that, because of the end-to-end nature of SimFlow, REPA applied to SimFlow naturally becomes REPA-E, where REPA gradients flow from the NF to the VAE encoder.

4.3 Working mechanism

Why does a fixed variance improve NF generation? First, our VAE is more robust to imperfect predictions from the generative model. We use different VAEs to reconstruct the 50K validation images in ImageNet 256×256 with increasing noise level on the latent, and then measure the reconstruct quality. Figure 3(a) shows that while a VAE with learnable variance achieves the best reconstruction quality when there is no noise on the latent, VAE with a large and fixed variance is more robust to noise. Thus, when NFs generate imperfect latent, our VAE can still decode good images. **Second**, we linearly interpolate the latents from two images and visualize the reconstruction results of the interpolation points. As seen in Figure 3(b), reconstruction results are better for the VAE with fixed variance, indicating that the latent space of our VAEs

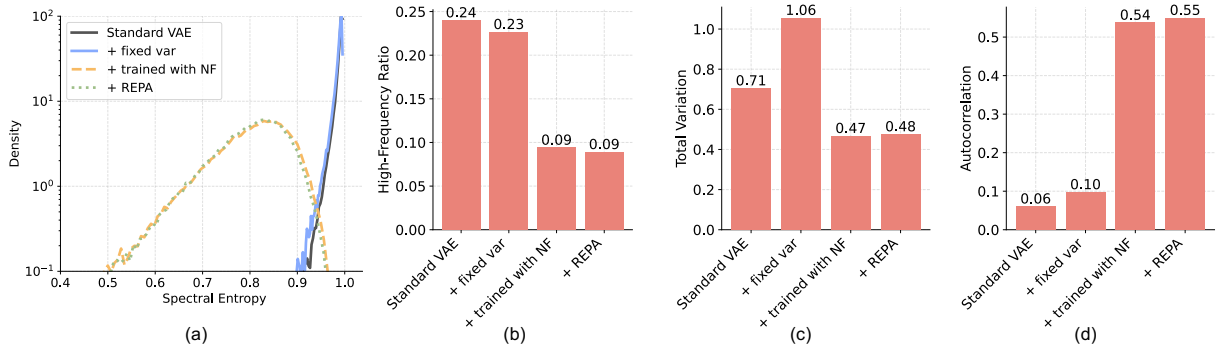


Figure 4 End-to-end training makes latent space more suitable for developing generative models. (a) Spectral entropy measures the randomness of frequency components; lower values indicate simpler data distributions in the frequency domain. (b) Ratio of high-frequency components. (c) Total variation captures the overall local changes across tokens; lower values imply smoother latents. (d) Autocorrelation reflects how similar a token sequence is to a shifted version of itself; higher autocorrelation indicates stronger spatial consistency.

is smooth and easy for NFs to learn. Note that, while large variance makes the VAE more robust, it may over-smooth the latent space and limit the reconstruction and generation quality. Thus, a moderate variance performs overall the best (see Section 5.3).

Why does fixed variance avoid latent collapse? Leng et al. [33] observe latent space collapse when they naively train DiT and VAE together. We observe the same phenomenon on latent NFs. The key reason is that the loss of generative models encourages the latent variables \mathbf{x} of different images to be close to each other. When the latent variance becomes smaller, the MSE loss term for DiTs or NFs is reduced, providing a shortcut for optimization and resulting in the latent collapse.

As discussed in Section 4.1, our encoder with fixed variance can be considered as a predicted mean μ plus noise: $\mathbf{x} = \mu + \epsilon, \epsilon \sim \mathcal{N}(\mathbf{0}, \sigma^2 \mathbf{I})$. If μ of different images were close to each other, the differences in μ would be overwhelmed by noise ϵ , making it hard to reconstruct images. To maintain good reconstruction quality, the system thus tends not to shrink the latent variation as much as naive end-to-end training, allowing for effective end-to-end training. We show similar effects of other noise design in Section 5.3.

How does end-to-end training help? Prior works explore what VAE latent space is suitable for training a generative model, especially for diffusion models [54, 66, 67]. Based on SimFlow, we present a new perspective: if we jointly train VAE with a generative model, will the latent space become more suitable for generation?

To answer this, we use different statistics to analyze latent space. As shown in Figure 4, the latent space of end-to-end training has lower spectral entropy and less high-frequency components, making it easier for generative models to fit the distribution [54]. Moreover, tokens have lower total variation and higher autocorrelation. This means the token sequence is more suitable for autoregressive modeling. Because our NF is based on AF, the latent space is therefore expected to be more favorable for NF modeling.

4.4 Revisit classifier-free guidance for NFs

CFG [21] significantly improves the performance of diffusion models, by using unconditional outputs to push the class-conditional predictions. This technique has been applied to NFs recently [17, 70]. TARFlow [70] does an early exploration but their method lacks theoretical foundation. STARFlow [17] carefully designs CFG for NFs based on mathematical proof, but their CFG can only be applied on the last NF block.

Inspired by the denoising step in TARFlow [70], we run STARFlow CFG first to generate tokens and then derive a score-based step on the generated tokens, *i.e.*,

$$\tilde{\mathbf{x}} = \mathbf{x} + \gamma(\nabla_{\mathbf{x}} \log p_{\text{NF}}(\mathbf{x}|c) - \nabla_{\mathbf{x}} \log p_{\text{NF}}(\mathbf{x}|\phi)), \quad (6)$$

where $\nabla_{\mathbf{x}} \log p_{\text{NF}}(\mathbf{x}|c)$ and $\nabla_{\mathbf{x}} \log p_{\text{NF}}(\mathbf{x}|\phi)$ are the gradients of the NF with and without class labels c , respectively. γ controls the step size. This step leverages the full distribution modeled by the NF and utilizes

Table 1 Class-conditional performance on ImageNet 256×256 . Methods requiring external pretrained models (e.g., DINOv2-B) for alignment are highlighted in blue.

Method	Epochs	#Params	VAE		W/o guidance				W/ guidance			
			rFID↓	PSNR↑	gFID↓	IS↑	Prec.↑	Rec.↑	gFID↓	IS↑	Prec.↑	Rec.↑
<i>Pixel Space</i>												
ADM [7]	400	554M	-	-	10.94	101.0	0.69	0.63	3.94	215.8	0.83	0.53
RIN [25]	480	410M	-	-	3.42	182.0	-	-	-	-	-	-
PixelFlow [5]	320	677M	-	-	-	-	-	-	1.98	282.1	0.81	0.60
PixNerd [63]	160	700M	-	-	-	-	-	-	2.15	297.0	0.79	0.59
SiD2 [22]	1280	-	-	-	-	-	-	-	1.38	-	-	-
TARFlow [70]	320	1.4B	-	-	-	-	-	-	4.69	-	-	-
JetFormer [60]	500	2.8B	-	-	-	-	-	-	6.64	-	0.69	0.56
FARMER [74]	320	1.9B	-	-	-	-	-	-	3.60	269.2	0.81	0.51
<i>Latent Autoregressive</i>												
VAR [59]	350	2.0B	-	-	1.92	323.1	0.82	0.59	1.73	350.2	0.82	0.60
MAR [35]	800	943M	0.53	26.18	2.35	227.8	0.79	0.62	1.55	303.7	0.81	0.62
xAR [48]	800	1.1B	0.53	26.18	-	-	-	-	1.24	301.6	0.83	0.64
<i>Latent Diffusion</i>												
DiT [45]	1400	675M	0.61	24.98	9.62	121.5	0.67	0.67	2.27	278.2	0.83	0.57
MaskDiT [75]	1600	675M	0.61	24.98	5.69	177.9	0.74	0.60	2.28	276.6	0.80	0.61
SiT [37]	1400	675M	0.61	24.98	8.61	131.7	0.68	0.67	2.06	270.3	0.82	0.59
MDTv2 [12]	1080	675M	0.61	24.98	-	-	-	-	1.58	314.7	0.79	0.65
REPA [69]	800	675M	0.61	24.98	5.78	158.3	0.70	0.68	1.29	306.3	0.79	0.64
VA-VAE [67]	800	675M	0.28	26.32	2.17	205.6	0.77	0.65	1.35	295.3	0.79	0.65
DDT [64]	400	675M	0.61	24.98	6.27	154.7	0.68	0.69	1.26	310.6	0.79	0.65
REPA-E [33]	800	675M	0.28	26.25	1.69	219.3	0.77	0.67	1.12	302.9	0.79	0.66
RAE [73]	800	839M	0.57	18.86	1.51	242.9	0.79	0.63	1.13	262.6	0.78	0.67
<i>Latent Normalizing Flows</i>												
STARFlow [17]	320	1.4B	2.73	-	-	-	-	-	2.40	-	-	-
SimFlow	160	1.4B	1.21	23.07	13.72	105.2	0.67	0.62	2.15	276.8	0.83	0.57
SimFlow + REPA-E	160	1.4B	1.08	23.17	10.13	124.7	0.71	0.61	1.91	284.4	0.82	0.60

all NF blocks, rather than only the final one, thereby further improving the generation quality over the CFG method in STARFlow. We will compare our CFG with STARFlow in Section 5.2.

5 Experiments

5.1 Implementation details

Experiments are conducted on the ImageNet 256×256 and 512×512 generation tasks [6]. We report gFID [20], IS [51], Precision, and Recall for generation [7]. Besides, rFID, PSNR [24], LPIPS [71], and SSIM [65] are reported for VAE reconstruction evaluation.

We use the MAR VAE architecture [35, 50] and TARFlow as the basic NF model. Both VAE and NF are trained from scratch. Following STARFlow, we use a deep-shallow architecture. Specifically, the NF model has six blocks with 1152 hidden dimensions. The first five blocks have two layers while the last deep block has 46 layers. Unless stated otherwise, SimFlow is trained for 80 epochs with a global batch size of 256 and a constant learning rate of 1.0×10^{-4} . In Table 1, we extend the training with extra 80 epochs to get further improved performance, where the learning rate reduces from 1.0×10^{-4} to 1.0×10^{-6} at a cosine rate like STARFlow. Details are presented in Section B.

5.2 Main evaluation

Comparison with state-of-the-art methods on ImageNet 256×256 . Results are shown in Table 1. SimFlow achieves a gFID of 2.15, significantly outperforming the prior NF method STARFlow (gFID=2.40). Note that STARFlow is trained for 320 epochs while SimFlow is trained for 160 epochs. Our jointly-trained VAE has better reconstruction quality (rFID=1.21) than STARFlow (rFID=2.73). Besides, SimFlow surpasses a representative diffusion model, DiT [45]. Although SimFlow needs more parameters, the convergence rate is more than 8 times faster than DiT.

Table 2 Class-conditional performance on ImageNet 512×512. SimFlow with REPA-E achieves better performance than DiT and STARFlow on generating higher-resolution images.

Method	#Params	gFID↓	IS↑	Prec.↑	Rec.↑
BigGAN-deep [2]	158M	8.43	177.9	0.88	0.29
StyleGAN-XL [52]	-	2.41	267.8	0.77	0.52
VAR [59]	2.3B	2.63	303.2	-	-
MAGVIT-v2 [68]	307M	1.91	324.3	-	-
MAR [35]	481M	1.73	279.9	-	-
XAR [48]	608M	1.70	281.5	-	-
ADM [7]	731M	3.85	221.7	0.84	0.53
SiD2	-	1.50	-	-	-
DiT [45]	674M	3.04	240.8	0.84	0.54
SiT [37]	674M	2.62	252.2	0.84	0.57
DiffiT [19]	-	2.67	252.1	0.83	0.55
REPA [69]	675M	2.08	274.6	0.83	0.58
DDT [64]	675M	1.28	305.1	0.80	0.63
EDM2 [26]	1.5B	1.25	-	-	-
RAE [73]	839M	1.13	259.6	0.80	0.63
STARFlow [17]	1.4B	3.00	-	-	-
SimFlow + REPA-E	1.4B	2.74	304.9	0.81	0.57

With REPA-E, SimFlow establishes the new state-of-the-art performance among NFs (gFID 1.91). REPA-E not only improves the generation quality in terms of gFID but also the reconstruction performance of VAE, with better rFID and PSNR. It indicates that the guidance from a pretrained model is helpful for building a better latent space, benefiting both the training of VAEs and NFs.

Comparison with state-of-the-art methods on ImageNet 512×512. Results are summarized in Table 2. SimFlow with REPA-E also works on higher resolution images and significantly surpasses STARFlow. Sample images generated from SimFlow are shown in Figure 6.

Effectiveness of end-to-end training. We present results in Figure 5. Specifically, we train a normal VAE with fixed variance and then train the NF model without updating the VAE at all, denoted as ‘Fixed var’ under the ‘Frozen VAE’ category. It is clear that our method ‘Fixed var’ under ‘End-to-end’ training significantly outperforms the other (gFID = 16.97 vs. gFID 67.41). Only setting a fixed variance is not enough. The end-to-end training makes the latent space significantly more suitable for generation. Moreover, we apply noise-augmented training [17] with encoder frozen (as in STARFlow) and end-to-end training, respectively. As seen in Figure 5, end-to-end training also obtains lower gFID, indicating its effectiveness.

Comparing fixed variance with noise augmentation under end-to-end training. As shown in Figure 5, fixed variance yields lower gFID (16.97 vs. 20.01). This demonstrates that fixing variance is a useful technique: it simplifies the pipeline while having competitive performance. Here, we do not claim our method is superior to noise augmentation because they essentially share similar principles, *i.e.*, perturbing the latents. We speculate that noise augmentation would have close performance in end-to-end training if we train the model longer or tune the hyperparameters.

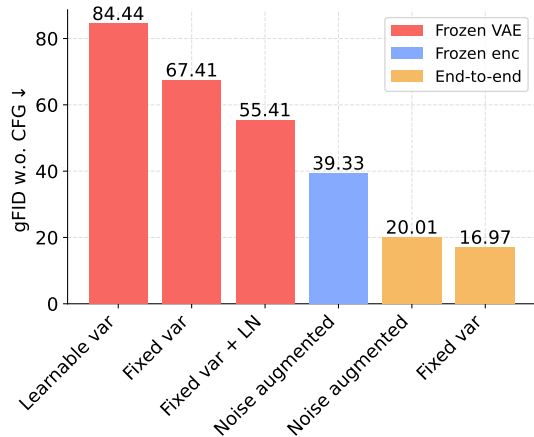


Figure 5 Variant studies. ‘Frozen VAE’ means both VAE encoder and decoder are frozen during training. ‘Frozen enc’ means the decoder is trained. ‘End-to-end’ means VAE encoder and decoder, and the NF are jointly trained from scratch. ‘Learnable var’ means the variance is predicted by the VAE, while ‘Fixed var’ is our method with $\bar{\sigma}^2 = 0.5^2$. ‘LN’ denotes applying a layer normalization on the VAE encoder. ‘Noise augmented’ indicates adding Gaussian noise to VAE latents as done by Gu et al. [17].

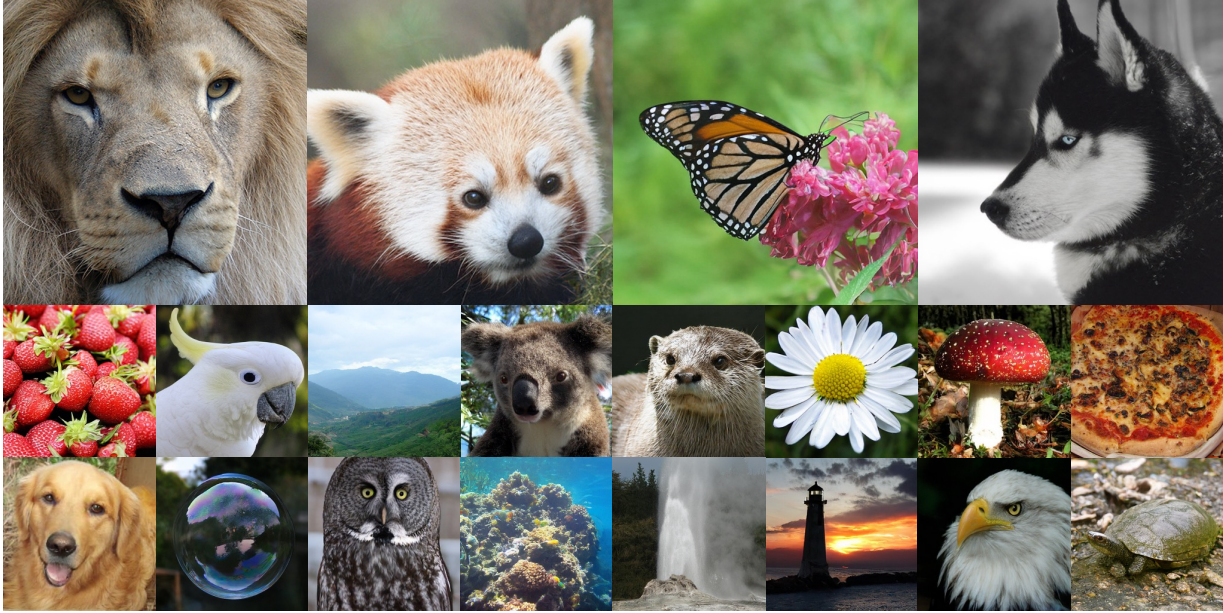


Figure 6 Qualitative Results. We show selected examples generated by SimFlow + REPA-E on ImageNet.

Reconstruction vs. generation. The best reconstruction results are achieved by learnable variance (see Section C.1). However, Figure 5 shows that learnable variance does not necessarily mean better generation. Our observation is consistent with prior works [67, 73], but from a different perspective of fixing or training the variance term in VAE.

Comparing the revised CFG method with STARFlow CFG [17]. We run STARFlow CFG first to generate tokens and then derive a score-based step, Eq. 6 on the tokens. As demonstrated in Figure 7, with $\gamma = 0.25$, our CFG significantly improves the optimal generation quality. We note that our CFG introduces only a mild increase in inference time compared to STARFlow (see Section C.3).

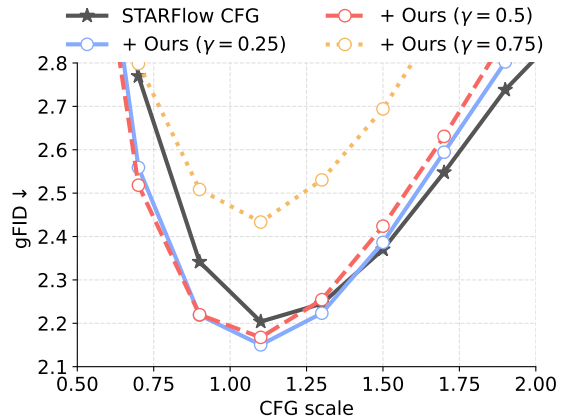


Figure 7 CFG method comparison. Our CFG method in Eq. 6 improves the best point over the STARFlow CFG [17].

5.3 Further analysis

Comparing different latent dimensions. Table 3 presents the performance of different VAE latent dimensions. Because we enforce a large and constant variance ($\bar{\sigma}^2 = 0.5^2$), a low latent dimension such as 16 cannot preserve sufficient information. In contrast, a high dimension such as 128, while benefiting reconstruction, would make it challenging for NF modeling. The best trade-off is 64-dimensional.

Table 3 Comparison of different latent dimensions. The best trade-off is 64-dimensional. The best results are shown in bold, and the default setting is highlighted in red.

Dim	rFID↓	PSNR↑	LPIPS↓	SSIM↑	gFID w.o. CFG↓	gFID w. CFG↓
16	4.98	19.94	0.327	0.45	11.00	3.55
32	2.60	21.42	0.274	0.51	12.77	2.61
64	1.49	23.01	0.222	0.59	21.44	2.53
128	0.86	24.61	0.183	0.66	33.43	3.62

Comparing different variance values. From Table 4, $\bar{\sigma}^2 = 0.5^2$ generally results in good reconstruction and generation quality. We notice that larger variance accelerates convergence because the latent space is smoother, but reduces the upper bound of the final performance. Overall, the performance of SimFlow is stable across a wide range of variance.

Table 4 Comparing different levels of variance. A moderate variance $\bar{\sigma}^2 = 0.5^2$ performs the best. The superior results are shown in bold, and the default setting is highlighted in yellow.

Var	rFID↓	PSNR↑	LPIPS↓	SSIM↑	gFID w.o. CFG↓	gFID w. CFG↓
0.1 ²	1.90	22.61	0.238	0.57	25.54	3.01
0.25 ²	1.55	22.94	0.225	0.58	21.35	2.57
0.5 ²	1.49	23.01	0.222	0.59	21.44	2.53
0.75 ²	1.54	22.88	0.224	0.59	17.76	2.39
1.0	1.76	22.60	0.231	0.58	19.36	2.66

Comparing different model sizes. In Table 5, scaling up NFs improves both the reconstruction and generation quality. A small NF cannot fit a complex latent distribution, and thus, the encoder tends to maintain a simple latent space, sacrificing the reconstruction quality. When the NF is larger and more expressive, generation quality is improved. Meanwhile, the encoder can embed more information into latents, enhancing reconstruction quality as well.

Table 5 Comparing different model sizes. Large NFs improve both the reconstruction and generation quality. The best results are shown in bold, and the default setting is highlighted in gray.

Model	#Params	rFID↓	PSNR↑	LPIPS↓	SSIM↑	gFID w.o. CFG↓	gFID w. CFG↓
S	37M	1.70	22.81	0.230	0.58	65.57	15.34
B	141M	1.66	22.89	0.226	0.58	52.77	9.72
L	475M	1.52	22.95	0.224	0.59	33.53	3.72
XL	695M	1.51	22.99	0.224	0.59	28.60	3.51
XXL	1.4B	1.49	23.01	0.222	0.59	21.44	2.53

Comparison of different ways of adding noise to latent \mathbf{x} . We test different latent noise discussed in prior works [40, 46, 66]. Specifically, we train VAEs with NFs for 100K iterations with these perturbations. As we expect in Section 4.3, Table 6 shows that all these methods avoid collapse during end-to-end training. Note that these perturbations have different strengths in removing information in latents, leading to different performance. If we tune the weights of the strengths of these methods, they should lead to similar results, which we leave for future exploration.

Table 6 Comparison of different ways of adding noise to latent \mathbf{x} . All these ways enable end-to-end training. Our method ‘Additive’ performs the best and is highlighted in green.

Noise	Equation	rFID↓	PSNR↑	gFID w.o. CFG↓
No noise	$\mathbf{x}' = \mathbf{x}$			Collapse
Linear	$\mathbf{x}' = t\mathbf{x} + (1-t)\epsilon$	8.54	19.74	71.0
Slerp	$\mathbf{x}' = t\mathbf{x} + \sqrt{1-t^2}\epsilon$	5.56	20.63	49.7
Additive	$\mathbf{x}' = \mathbf{x} + \epsilon$	2.90	22.22	39.6

Effectiveness of SimFlow methods applied to diffusion models. We perform a preliminary study by jointly training VAE and SiT [37]. We choose the VAE in LDM [50] and use the 32- and 64-dimensional checkpoints from Yao et al. [67], which were trained for 50 epochs. We compare 1) SiT trained for 50 epochs with the pretrained VAE frozen, and 2) jointly train SiT and a new VAE for 50 epochs from scratch. Table 7 shows our method also speeds up the training of diffusion models and achieves better generation quality after the same iterations. With 80 epochs of end-to-end training, the performance is further improved. End-to-end diffusion model training is a promising future direction.

Table 7 Applying fixed variance to end-to-end training of diffusion models and VAEs. The colored rows indicate our methods with fixed variance in VAEs.

VAE dim	VAE epochs	Diff. epochs	Joint	rFID↓	PSNR↑	gFID w.o. CFG↓
32	50	50	✗	0.26	28.59	20.36
32	50	50	✓	1.26	21.86	17.70 (-2.66)
64	50	50	✗	0.17	31.03	28.34
64	50	50	✓	0.82	22.83	19.10 (-9.24)
64	80	80	✓	0.76	23.10	13.91

6 Conclusion

This paper presents SimFlow, an end-to-end training framework for latent NFs by simply fixing the VAE variance. This makes latent space smoother and helps NFs generalize better when sampling, without needing extra noise schedules or denoising steps. Experiments show that SimFlow improves generation quality and speeds up training compared to existing NF methods. Future work will expand this framework to text-to-image training and explore a second-stage training with the VAE fixed after joint training.

Appendix

A Training objectives

A.1 VAE ELBO

A standard VAE [28] consists of an encoder q_ψ and a decoder p_ω . Given an image \mathbf{i} , the encoder predicts mean $\boldsymbol{\mu}$ and variance $\boldsymbol{\sigma}^2$ of a Gaussian distribution $\mathcal{N}(\boldsymbol{\mu}, \text{diag}(\boldsymbol{\sigma}^2))$. A latent variable \mathbf{x} (a set of tokens) is sampled from $\mathcal{N}(\boldsymbol{\mu}, \text{diag}(\boldsymbol{\sigma}^2))$. The decoder is trained to reconstruct the image \mathbf{i} from \mathbf{x} . The log likelihood $\log p(\mathbf{i})$ for VAEs can be decomposed as follows [4]:

$$\log p(\mathbf{i}) = \underbrace{\mathbb{E}_{q_\psi(\mathbf{x}|\mathbf{i})} \left[\log \frac{p(\mathbf{i}, \mathbf{x})}{q_\psi(\mathbf{x}|\mathbf{i})} \right]}_{\stackrel{\text{def}}{=} \text{ELBO}(\mathbf{i})} + \mathbb{D}_{\text{KL}}(q_\psi(\mathbf{x}|\mathbf{i}) \| p(\mathbf{x}|\mathbf{i})). \quad (7)$$

To prove the preceding equation, first, we use the proxy $q_\psi(\mathbf{x}|\mathbf{i})$ to poke around $p(\mathbf{i})$.

$$\log p(\mathbf{i}) = \log p(\mathbf{i}) \times \underbrace{\int q_\psi(\mathbf{x}|\mathbf{i}) d\mathbf{x}}_{=1} \quad (\text{multiply } 1) \quad (8)$$

$$= \int \log p(\mathbf{i}) \times q_\psi(\mathbf{x}|\mathbf{i}) d\mathbf{x} \quad (9)$$

$$= \mathbb{E}_{q_\psi(\mathbf{x}|\mathbf{i})} [\log p(\mathbf{i})], \quad (10)$$

where the last equality is the fact that $\int a \times p_Z(z) dz = \mathbb{E}[a] = a$ for any random variable Z and a scalar a . Then, we use Bayes theorem, *i.e.*, $p(\mathbf{i}, \mathbf{x}) = p(\mathbf{x}|\mathbf{i})p(\mathbf{i})$:

$$\mathbb{E}_{q_\psi(\mathbf{x}|\mathbf{i})} [\log p(\mathbf{i})] \quad (11)$$

$$= \mathbb{E}_{q_\psi(\mathbf{x}|\mathbf{i})} \left[\log \frac{p(\mathbf{i}, \mathbf{x})}{p(\mathbf{x}|\mathbf{i})} \right] \quad (\text{Bayes Theorem}) \quad (12)$$

$$= \mathbb{E}_{q_\psi(\mathbf{x}|\mathbf{i})} \left[\log \frac{p(\mathbf{i}, \mathbf{x})}{p(\mathbf{x}|\mathbf{i})} \times \frac{q_\psi(\mathbf{x}|\mathbf{i})}{q_\psi(\mathbf{x}|\mathbf{i})} \right] \quad (13)$$

$$= \underbrace{\mathbb{E}_{q_\psi(\mathbf{x}|\mathbf{i})} \left[\log \frac{p(\mathbf{i}, \mathbf{x})}{q_\psi(\mathbf{x}|\mathbf{i})} \right]}_{\text{ELBO}} + \underbrace{\mathbb{E}_{q_\psi(\mathbf{x}|\mathbf{i})} \left[\log \frac{q_\psi(\mathbf{x}|\mathbf{i})}{p(\mathbf{x}|\mathbf{i})} \right]}_{\mathbb{D}_{\text{KL}}(q_\psi(\mathbf{x}|\mathbf{i}) \| p(\mathbf{x}|\mathbf{i}))}, \quad (14)$$

where we recognize that the first term is exactly ELBO, whereas the second term is exactly the KL divergence. Comparing Eq. 14 with Eq. 10, we get Eq. 7. Because the KL divergence is always non-negative, we have

$$\log p(\mathbf{i}) \geq \mathbb{E}_{q_\psi(\mathbf{x}|\mathbf{i})} \left[\log \frac{p(\mathbf{i}, \mathbf{x})}{q_\psi(\mathbf{x} | \mathbf{i})} \right]. \quad (15)$$

Moreover, we can decompose the ELBO as follows:

$$\text{ELBO}(\mathbf{i}) \quad (16)$$

$$\stackrel{\text{def}}{=} \mathbb{E}_{q_\psi(\mathbf{x}|\mathbf{i})} \left[\log \frac{p(\mathbf{i}, \mathbf{x})}{q_\psi(\mathbf{x} | \mathbf{i})} \right] \quad (17)$$

$$= \mathbb{E}_{q_\psi(\mathbf{x}|\mathbf{i})} \left[\log \frac{p(\mathbf{i} | \mathbf{x})p(\mathbf{x})}{q_\psi(\mathbf{x} | \mathbf{i})} \right] \quad (18)$$

$$= \mathbb{E}_{q_\psi(\mathbf{x}|\mathbf{i})} \left[\underbrace{\log p_\omega(\mathbf{i} | \mathbf{x})}_{\text{Reconstruction}} + \underbrace{\log p(\mathbf{x})}_{\text{Prior}} - \underbrace{\log q_\psi(\mathbf{x} | \mathbf{i})}_{\text{Entropy}} \right], \quad (19)$$

where we replaced the inaccessible $p(\mathbf{i} | \mathbf{x})$ by its proxy $p_\omega(\mathbf{i} | \mathbf{x})$. The prior term is usually chosen as the normal distribution $\mathcal{N}(\mathbf{0}, \mathbf{I})$ in standard VAEs. In SimFlow, we replace the prior term with the NF-modeled probability (Section A.2) and the entropy term simplifies to a constant (Section A.3).

A.2 NF loss

Latent NFs map the VAE latent distribution into the normal distribution $\mathbf{z} \sim p_0(\mathbf{z})$, via learning an invertible function f_θ . NFs are trained with maximum likelihood estimation, following the change of variable formula:

$$\max_{\theta} \mathbb{E}_{\mathbf{x} \sim p_{\text{latent}}} \log p_{\text{NF}}(\mathbf{x}; \theta). \quad (20)$$

$$= \mathbb{E}_{\mathbf{x} \sim p_{\text{latent}}} \left[\log p_0(f_\theta(\mathbf{x})) + \log \left| \det \left(\frac{\partial f_\theta(\mathbf{x})}{\partial \mathbf{x}} \right) \right| \right] \quad (21)$$

$$= \mathbb{E}_{\mathbf{x} \sim p_{\text{latent}}} \left[-\frac{1}{2} \|f_\theta(\mathbf{x})\|_2^2 + \log \left| \det \left(\frac{\partial f_\theta(\mathbf{x})}{\partial \mathbf{x}} \right) \right| \right], \quad (22)$$

where Eq. 22 leverages the log-likelihood of the normal distribution and removes terms independent of \mathbf{x} .

We build our study on STARFlow [17] and thus, use the same NF loss with TARFlow [70]. The forward and inverse processes of a TARFlow block are:

$$\mathbf{z}_d = \frac{\mathbf{x}_d - \beta_\theta(\mathbf{x}_{<d})}{\alpha_\theta(\mathbf{x}_{<d})}, \mathbf{x}_d = \beta_\theta(\mathbf{x}_{<d}) + \alpha_\theta(\mathbf{x}_{<d}) \cdot \mathbf{z}_d, \quad (23)$$

where $d \in [1, D]$ denotes the token id. The Jacobian term in Eq. 2 becomes extremely simple:

$$\log \left| \det \left(\frac{\partial f_\theta(\mathbf{x})}{\partial \mathbf{x}} \right) \right| = - \sum_{d=1}^D \log \alpha_\theta(\mathbf{x}_{<d}). \quad (24)$$

TARFlow [70] stacks T blocks whose autoregressive ordering alternates from one layer to the next, *e.g.*, in the first layer, from left to right, and in the next layer, from right to left. Training is performed for all blocks:

$$\max_{\theta} \mathbb{E}_{\mathbf{x} \sim p_{\text{latent}}} \left[-\frac{1}{2} \|f_\theta(\mathbf{x})\|_2^2 - \sum_{t=1}^T \sum_{d=1}^D \log \alpha_\theta^t(\mathbf{x}_{<d}^t) \right]. \quad (25)$$

A.3 Constant entropy term in SimFlow

Now, we analyze the entropy term in Eq. 19.

$$-\mathbb{E}_{q_\psi(\mathbf{x}|\mathbf{i})} [\log q_\psi(\mathbf{x} | \mathbf{i})] \quad (26)$$

$$= -\mathbb{E}_{q_\psi(\mathbf{x}|\mathbf{i})} \left[\log \prod_{i=1}^N \frac{1}{\sigma_i \sqrt{2\pi}} \exp\left(-\frac{1}{2} \left(\frac{x_i - \mu_i}{\sigma_i}\right)^2\right) \right] \quad (27)$$

$$= -\mathbb{E}_{q_\psi(\mathbf{x}|\mathbf{i})} \left[-\sum_{i=1}^N \left(\log(\sigma_i \sqrt{2\pi}) + \frac{1}{2} \left(\frac{x_i - \mu_i}{\sigma_i}\right)^2 \right) \right] \quad (28)$$

$$= \frac{1}{2} \sum_{i=1}^N \log(2\pi\sigma_i^2) + \frac{1}{2} \mathbb{E}_{q_\psi(\mathbf{x}|\mathbf{i})} \left[\sum_{i=1}^N \left(\frac{x_i - \mu_i}{\sigma_i}\right)^2 \right]. \quad (29)$$

Note that

$$\mathbb{E}_{q_\psi(\mathbf{x}|\mathbf{i})} \left[\sum_{i=1}^N \left(\frac{x_i - \mu_i}{\sigma_i}\right)^2 \right] \quad (30)$$

$$= \sum_{i=1}^N \mathbb{E}_{x_i \sim \mathcal{N}(\mu_i, \sigma_i^2)} \left[\left(\frac{x_i - \mu_i}{\sigma_i}\right)^2 \right] \quad (31)$$

$$= \sum_{i=1}^N \mathbb{E}_{x_i \sim \mathcal{N}(\mu_i, \sigma_i^2)} \left[\frac{(x_i - \mu_i)^2}{\sigma_i^2} \right] \quad (32)$$

$$= N \quad (\text{Var}(x) = \mathbb{E}[(x - \mu)^2]). \quad (33)$$

Thus,

$$-\mathbb{E}_{q_\psi(\mathbf{x}|\mathbf{i})} [\log q_\psi(\mathbf{x} | \mathbf{i})] = \frac{1}{2} \sum_{i=1}^N \log(2\pi\sigma_i^2) + \frac{1}{2} N. \quad (34)$$

Because we set all σ_i to be a fixed value, the entropy term also becomes a constant in SimFlow.

A.4 Objective of end-to-end training

Last, we combine Eq.19, Eq.25, with Eq. 34 and we omit the constant entropy term. The objective of our end-to-end training is presented as follows:

$$\max_{\boldsymbol{\theta}, \boldsymbol{\psi}, \boldsymbol{\omega}} \mathbb{E}_{\mathbf{i} \sim p_{\text{data}}} \mathbb{E}_{\mathbf{x} \sim q_\psi(\mathbf{x}|\mathbf{i})} [\log p_\omega(\mathbf{i} | \mathbf{x}) + \log p_{\text{NF}}(\mathbf{x}; \boldsymbol{\theta})] \quad (35)$$

$$= \mathbb{E}_{\mathbf{i} \sim p_{\text{data}}} \mathbb{E}_{\mathbf{x} \sim q_\psi(\mathbf{x}|\mathbf{i})} \left[\log p_\omega(\mathbf{i} | \mathbf{x}) - \frac{1}{2} \|f_{\boldsymbol{\theta}}(\mathbf{x})\|_2^2 - \sum_{t=1}^T \sum_{d=1}^D \log \alpha_{\boldsymbol{\theta}}^t(\mathbf{x}_{<d}^t) \right]. \quad (36)$$

Note that the reconstruction loss (the first term) is typically averaged at the pixel level, while the NF loss terms (the second and third terms) are normalized at the latent feature level. Therefore, in the specific implementation of our codes, we average the loss terms at different levels. We do not further tune the weight of each term. Besides, we also add perceptual loss and adversarial loss [14] for VAE training [50].

B Implementation details

VAE. We employ the MAR VAE architecture [35], which is adapted from the LDM VAE [50] and comprises approximately 67 million parameters. We maintain most of the original hyperparameters from Li et al. [35], modifying only the latent dimension (*e.g.*, 16, 32, or 64). The patch size remains fixed at 16. Additionally, following recent findings that highlight the benefits of normalization layers in VAE encoders [73], we also apply a Layer Normalization to each token independently. This normalizes the tokens into a constrained space and improves the gFID score by about 0.15.

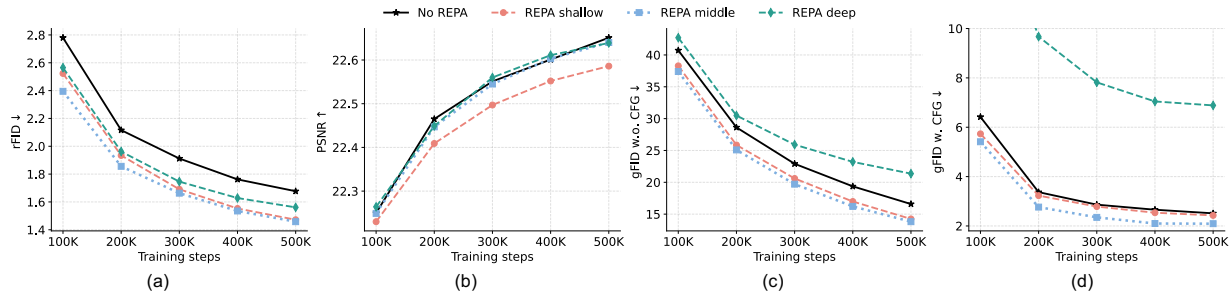


Figure 8 Effects of REPA-E on SimFlow. Aligning a middle block leads to the most consistent gains.

NF. We utilize TARFlow [70] as the foundational NF model, because it is the latest open-source NF model. We implement two upgrades to TARFlow. First, we adopt a deep-shallow architecture, following Gu et al. [17], where the final block contains multiple layers while all other blocks consist of only two layers. Second, we incorporate the adaLN-Zero mechanism into the NF for class conditioning, following the design of DiT [45] and SiT [37]. A detailed configuration of our models is provided in Table 8 and the training configuration is presented in Table 9.

REPA-E. During training, we use a three-layer multilayer perceptron (MLP) to align the hidden features from an NF block with features extracted by a frozen DINOv2-B model [3]. The MLP itself is trainable. As detailed in Section C.2, we compare three different choices for the NF block to align and find that aligning a middle block within the NF model yields the best performance.

C Additional experiments

C.1 Variant studies

Table 10 presents detailed results of variants, which is partly visualized in Figure 5. The best reconstruction results are achieved by learnable variance (rFID 0.23) but it does not necessarily mean better generation (gFID 84.44). In comparison, while end-to-end training slightly degrades the reconstruction, the generation quality is significantly improved. Our observation is consistent with prior works [67, 73], but from a different perspective of fixing or training the variance term in VAEs.

C.2 Choice of NF blocks for REPA-E

We align different blocks of NFs: the first block, a middle block, or the last one. The results are shown in Figure 8. As seen, introducing alignment at shallow layers negatively affects the VAE reconstruction performance (lower PSNR), whereas applying alignment at deeper layers harms the generation quality. The reason is that aligning the first block mainly affects the VAE latents and only has a slight impact on NFs. Moreover, in the last block, we expect that data distribution is close to the noise distribution, so this block is not suitable for semantic understanding and alignment. As a result, aligning a middle block within the NF model leads to the most consistent gains.

Table 8 Model configurations for different sizes. Depth ‘2, 2, 2, 2, 2, x’ denote that each of the first five blocks consists of only two layers while the last block contains ‘x’ layers.

Model	#Params	Dim	Num-Heads	Depth
S	37M	384	6	2, 2, 2, 2, 2, 2
B	141M	768	12	2, 2, 2, 2, 2, 2
L	475M	1024	16	2, 2, 2, 2, 2, 14
XL	695M	1152	16	2, 2, 2, 2, 2, 18
XXL	1.4B	1152	16	2, 2, 2, 2, 2, 36

Table 9 Training configurations for SimFlow.

Warm-up epochs	0
Pretraining epochs	0
Stage-I	
Epochs	80
Learning rate	1.0×10^{-4}
Learning rate schedule	constant
Stage-II	
Epochs	80
Learning rate	$1.0 \times 10^{-4} \rightarrow 1.0 \times 10^{-6}$
Learning rate schedule	cosine rate
Stage-I and -II	
Image size	256 or 512
Optimizer	AdamW [36], $\beta_1, \beta_2 = 0.9, 0.999$
Batch size	256
Weight decay	0
EMA rate	0.9999
Max gradient norm	1.0
Class token drop (for CFG)	0.1
REPA-E	
REPA loss coef	1.0
Align depth	layer 1 at the block 3
Encoder	DINOv2-B [3]

Table 10 Variant studies. ‘Frozen VAE’ means both VAE encoder and decoder are frozen during training. ‘Frozen enc’ means the decoder is trained. ‘End-to-end’ means VAE encoder and decoder, and the NF are jointly trained from scratch. ‘Learnable var’ means the variance is predicted by the VAE, while ‘Fixed var’ is our method with $\sigma^2 = 0.5^2$. ‘LN’ denotes applying a layer normalization on the VAE encoder. ‘Noise’ indicates adding Gaussian noise to VAE latents as done by Gu et al. [17].

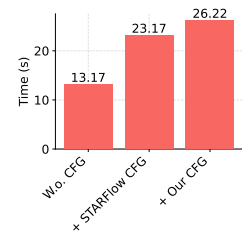
Config	Method	rFID↓	PSNR↑	gFID w.o. CFG↓
Frozen VAE	Learnable var	0.23	29.76	84.44
	Fixed var	0.40	27.54	67.41
	Fixed var + LN	1.07	24.43	55.41
Frozen Encoder	Noise	4.07	19.94	39.33
End-to-end	Noise	1.39	23.20	20.01
	Fixed var	1.76	22.61	16.97

C.3 Efficiency of our CFG method

We measure the average inference time of generating a batch of 256 images for SimFlow 1) without CFG, 2) with STARFlow CFG, and 3) with STARFlow + our CFG. As shown in the right figure, our method only mildly increases the inference time compared to the STARFlow CFG baseline.

C.4 Qualitative Results

Figures 9 to 12 present additional uncurated examples on ImageNet 256×256 with SimFlow+REPA-E. We follow the practice of Li and He [34].





class 012: house finch, linnet, *Carpodacus mexicanus*



class 014: indigo bunting, indigo finch, indigo bird, *Passerina cyanea*



class 042: agama



class 081: ptarmigan



class 107: jellyfish



class 108: sea anemone, anemone



class 110: flatworm, platyhelminth



class 117: chambered nautilus, pearly nautilus, nautilus



class 130: flamingo



class 279: Arctic fox, white fox, *Alopex lagopus*

Figure 9 *Uncurated* samples on ImageNet 256×256 using SimFlow + REPA-E conditioned on the specified classes. Unlike the common practice of visualizing with a higher CFG, here we show images using the CFG value that achieves the reported gFID of 1.91.



class 288: leopard, Panthera pardus



class 309: bee



class 349: bighorn, bighorn sheep, cimarron, Rocky Mountain bighorn



class 397: puffer, pufferfish, blowfish, globefish



class 425: barn



class 448: birdhouse



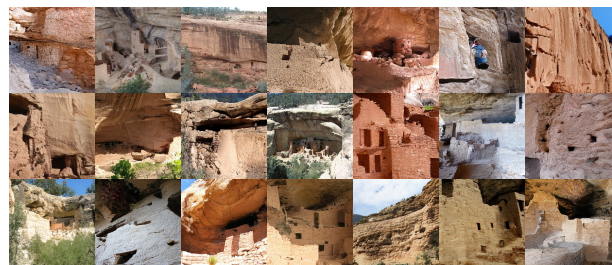
class 453: bookcase



class 458: brass, memorial tablet, plaque



class 495: china cabinet, china closet



class 500: cliff dwelling

Figure 10 *Uncurated* samples on ImageNet 256×256 using SimFlow + REPA-E conditioned on the specified classes. Unlike the common practice of visualizing with a higher CFG, here we show images using the CFG value that achieves the reported gFID of 1.91.



class 658: mitten



class 661: Model T



class 718: pier



class 724: pirate, pirate ship



class 725: pitcher, ewer



class 757: recreational vehicle, RV, R.V.



class 779: school bus



class 780: schooner



class 829: streetcar, tram, tramcar, trolley, trolley car



class 853: thatch, thatched roof

Figure 11 *Uncurated* samples on ImageNet 256×256 using SimFlow + REPA-E conditioned on the specified classes. Unlike the common practice of visualizing with a higher CFG, here we show images using the CFG value that achieves the reported gFID of 1.91.



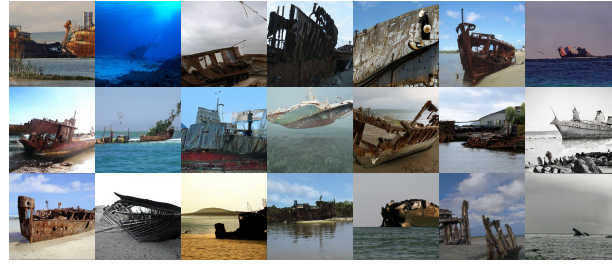
class 873: triumphal arch



class 900: water tower



class 911: wool, woolen, woollen



class 913: wreck



class 927: trifle



class 930: French loaf



class 946: cardoon



class 947: mushroom



class 975: lakeside, lakeshore



class 989: hip, rose hip, rosehip

Figure 12 *Uncurated* samples on ImageNet 256×256 using SimFlow + REPA-E conditioned on the specified classes. Unlike the common practice of visualizing with a higher CFG, here we show images using the CFG value that achieves the reported gFID of 1.91.

References

- [1] Fan Bao, Shen Nie, Kaiwen Xue, Yue Cao, Chongxuan Li, Hang Su, and Jun Zhu. All are worth words: A vit backbone for diffusion models. In Proceedings of the IEEE/CVF conference on computer vision and pattern recognition, pages 22669–22679, 2023.
- [2] Andrew Brock. Large scale gan training for high fidelity natural image synthesis. arXiv preprint arXiv:1809.11096, 2018.
- [3] Mathilde Caron, Hugo Touvron, Ishan Misra, Hervé Jégou, Julien Mairal, Piotr Bojanowski, and Armand Joulin. Emerging properties in self-supervised vision transformers. In Proceedings of the IEEE/CVF international conference on computer vision, pages 9650–9660, 2021.
- [4] Stanley Chan et al. Tutorial on diffusion models for imaging and vision. Foundations and Trends® in Computer Graphics and Vision, 16(4):322–471, 2024.
- [5] Shoufa Chen, Chongjian Ge, Shilong Zhang, Peize Sun, and Ping Luo. Pixelflow: Pixel-space generative models with flow. arXiv preprint arXiv:2504.07963, 2025.
- [6] Jia Deng, Wei Dong, Richard Socher, Li-Jia Li, Kai Li, and Li Fei-Fei. Imagenet: A large-scale hierarchical image database. In 2009 IEEE conference on computer vision and pattern recognition, pages 248–255. Ieee, 2009.
- [7] Prafulla Dhariwal and Alexander Nichol. Diffusion models beat gans on image synthesis. Advances in neural information processing systems, 34:8780–8794, 2021.
- [8] Laurent Dinh, David Krueger, and Yoshua Bengio. Nice: Non-linear independent components estimation. arXiv preprint arXiv:1410.8516, 2014.
- [9] Laurent Dinh, Jascha Sohl-Dickstein, and Samy Bengio. Density estimation using real nvp. In International Conference on Learning Representations, 2017.
- [10] Felix Draxler, Peter Sorrenson, Lea Zimmermann, Armand Rousselot, and Ullrich Köthe. Free-form flows: Make any architecture a normalizing flow. In International Conference on Artificial Intelligence and Statistics, pages 2197–2205. PMLR, 2024.
- [11] Felix Draxler, Stefan Wahl, Christoph Schnörr, and Ullrich Köthe. On the universality of volume-preserving and coupling-based normalizing flows. arXiv preprint arXiv:2402.06578, 2024.
- [12] Shanghua Gao, Pan Zhou, Ming-Ming Cheng, and Shuicheng Yan. Mdtv2: Masked diffusion transformer is a strong image synthesizer. arXiv preprint arXiv:2303.14389, 2023.
- [13] Robert Giaquinto and Arindam Banerjee. Gradient boosted normalizing flows. Advances in Neural Information Processing Systems, 33:22104–22117, 2020.
- [14] Ian Goodfellow, Jean Pouget-Abadie, Mehdi Mirza, Bing Xu, David Warde-Farley, Sherjil Ozair, Aaron Courville, and Yoshua Bengio. Generative adversarial networks. Communications of the ACM, 63(11):139–144, 2020.
- [15] Jiatao Gu, Ying Shen, Shuangfei Zhai, Yizhe Zhang, Navdeep Jaitly, and Joshua Susskind. Kaleido diffusion: Improving conditional diffusion models with autoregressive latent modeling. Advances in Neural Information Processing Systems, 37:5498–5527, 2024.
- [16] Jiatao Gu, Yuyang Wang, Yizhe Zhang, Qihang Zhang, Dinghuai Zhang, Navdeep Jaitly, Josh Susskind, and Shuangfei Zhai. Dart: Denoising autoregressive transformer for scalable text-to-image generation. arXiv preprint arXiv:2410.08159, 2024.
- [17] Jiatao Gu, Tianrong Chen, David Berthelot, Huangjie Zheng, Yuyang Wang, Ruixiang Zhang, Laurent Dinh, Miguel Angel Bautista, Josh Susskind, and Shuangfei Zhai. Starflow: Scaling latent normalizing flows for high-resolution image synthesis. arXiv preprint arXiv:2506.06276, 2025.
- [18] Jiatao Gu, Ying Shen, Tianrong Chen, Laurent Dinh, Yuyang Wang, Miguel Angel Bautista, David Berthelot, Josh Susskind, and Shuangfei Zhai. Starflow-v: End-to-end video generative modeling with normalizing flow. arXiv preprint arXiv:2511.20462, 2025.
- [19] Ali Hatamizadeh, Jiaming Song, Guilin Liu, Jan Kautz, and Arash Vahdat. Diffit: Diffusion vision transformers for image generation. In European Conference on Computer Vision, pages 37–55. Springer, 2024.

- [20] Martin Heusel, Hubert Ramsauer, Thomas Unterthiner, Bernhard Nessler, and Sepp Hochreiter. Gans trained by a two time-scale update rule converge to a local nash equilibrium. Advances in Neural Information Processing Systems, 30, 2017.
- [21] Jonathan Ho and Tim Salimans. Classifier-free diffusion guidance. arXiv preprint arXiv:2207.12598, 2022.
- [22] Emiel Hoogeboom, Thomas Mensink, Jonathan Heek, Kay Lamerigts, Ruiqi Gao, and Tim Salimans. Simpler diffusion (sid2): 1.5 fid on imagenet512 with pixel-space diffusion. arXiv preprint arXiv:2410.19324, 2024.
- [23] Chin-Wei Huang, David Krueger, Alexandre Lacoste, and Aaron Courville. Neural autoregressive flows. In International conference on machine learning, pages 2078–2087. PMLR, 2018.
- [24] Quan Huynh-Thu and Mohammed Ghanbari. Scope of validity of psnr in image/video quality assessment. Electronics letters, 44(13):800–801, 2008.
- [25] Allan Jabri, David Fleet, and Ting Chen. Scalable adaptive computation for iterative generation. arXiv preprint arXiv:2212.11972, 2022.
- [26] Tero Karras, Miika Aittala, Jaakko Lehtinen, Janne Hellsten, Timo Aila, and Samuli Laine. Analyzing and improving the training dynamics of diffusion models. In Proceedings of the IEEE/CVF Conference on Computer Vision and Pattern Recognition, pages 24174–24184, 2024.
- [27] Guolin Ke and Hui Xue. Hyperspherical latents improve continuous-token autoregressive generation. arXiv preprint arXiv:2509.24335, 2025.
- [28] Diederik P Kingma and Max Welling. Auto-encoding variational bayes. arXiv preprint arXiv:1312.6114, 2013.
- [29] Durk P Kingma and Prafulla Dhariwal. Glow: Generative flow with invertible 1x1 convolutions. Advances in neural information processing systems, 31, 2018.
- [30] Durk P Kingma, Tim Salimans, Rafal Jozefowicz, Xi Chen, Ilya Sutskever, and Max Welling. Improved variational inference with inverse autoregressive flow. Advances in neural information processing systems, 29, 2016.
- [31] Ivan Kobyzev, Simon JD Prince, and Marcus A Brubaker. Normalizing flows: An introduction and review of current methods. IEEE transactions on pattern analysis and machine intelligence, 43(11):3964–3979, 2020.
- [32] Theodoros Kouzelis, Ioannis Kakogeorgiou, Spyros Gidaris, and Nikos Komodakis. Eq-vae: Equivariance regularized latent space for improved generative image modeling. arXiv preprint arXiv:2502.09509, 2025.
- [33] Xingjian Leng, Jaskirat Singh, Yunzhong Hou, Zhenchang Xing, Saining Xie, and Liang Zheng. Repa-e: Unlocking vae for end-to-end tuning with latent diffusion transformers. arXiv preprint arXiv:2504.10483, 2025.
- [34] Tianhong Li and Kaiming He. Back to basics: Let denoising generative models denoise. arXiv preprint arXiv:2511.13720, 2025.
- [35] Tianhong Li, Yonglong Tian, He Li, Mingyang Deng, and Kaiming He. Autoregressive image generation without vector quantization. Advances in Neural Information Processing Systems, 37:56424–56445, 2024.
- [36] Ilya Loshchilov and Frank Hutter. Decoupled weight decay regularization. arXiv preprint arXiv:1711.05101, 2017.
- [37] Nanye Ma, Mark Goldstein, Michael S Albergo, Nicholas M Boffi, Eric Vanden-Eijnden, and Saining Xie. Sit: Exploring flow and diffusion-based generative models with scalable interpolant transformers. arXiv preprint arXiv:2401.08740, 2024.
- [38] Bálint Máté, Samuel Klein, Tobias Golling, and François Fleuret. Flowification: Everything is a normalizing flow. Advances in Neural Information Processing Systems, 35:35478–35489, 2022.
- [39] Emile Mathieu and Maximilian Nickel. Riemannian continuous normalizing flows. Advances in neural information processing systems, 33:2503–2515, 2020.
- [40] Viacheslav Meshchaninov, Egor Chibulatov, Alexander Shabalina, Aleksandr Abramov, and Dmitry Vetrov. Compressed and smooth latent space for text diffusion modeling. arXiv preprint arXiv:2506.21170, 2025.
- [41] Ziqi Pang, Tianyuan Zhang, Fujun Luan, Yunze Man, Hao Tan, Kai Zhang, William T Freeman, and Yu-Xiong Wang. Randar: Decoder-only autoregressive visual generation in random orders. In Proceedings of the Computer Vision and Pattern Recognition Conference, pages 45–55, 2025.

- [42] George Papamakarios, Theo Pavlakou, and Iain Murray. Masked autoregressive flow for density estimation. *Advances in neural information processing systems*, 30, 2017.
- [43] George Papamakarios, Eric Nalisnick, Danilo Jimenez Rezende, Shakir Mohamed, and Balaji Lakshminarayanan. Normalizing flows for probabilistic modeling and inference. *Journal of Machine Learning Research*, 22(57):1–64, 2021.
- [44] Massimiliano Patacchiola, Aliaksandra Shysheya, Katja Hofmann, and Richard E Turner. Transformer neural autoregressive flows. *arXiv preprint arXiv:2401.01855*, 2024.
- [45] William Peebles and Saining Xie. Scalable diffusion models with transformers. In *Proceedings of the IEEE/CVF International Conference on Computer Vision*, pages 4195–4205, 2023.
- [46] Kai Qiu, Xiang Li, Hao Chen, Jason Kuen, Xiaohao Xu, Jiuxiang Gu, Yinyi Luo, Bhiksha Raj, Zhe Lin, and Marios Savvides. Image tokenizer needs post-training. *arXiv preprint arXiv:2509.12474*, 2025.
- [47] Sucheng Ren, Qihang Yu, Ju He, Xiaohui Shen, Alan Yuille, and Liang-Chieh Chen. Flowar: Scale-wise autoregressive image generation meets flow matching. *arXiv preprint arXiv:2412.15205*, 2024.
- [48] Sucheng Ren, Qihang Yu, Ju He, Xiaohui Shen, Alan Yuille, and Liang-Chieh Chen. Beyond next-token: Next-x prediction for autoregressive visual generation. *arXiv preprint arXiv:2502.20388*, 2025.
- [49] Danilo Rezende and Shakir Mohamed. Variational inference with normalizing flows. In *International conference on machine learning*, pages 1530–1538. PMLR, 2015.
- [50] Robin Rombach, Andreas Blattmann, Dominik Lorenz, Patrick Esser, and Björn Ommer. High-resolution image synthesis with latent diffusion models. In *Proceedings of the IEEE/CVF conference on computer vision and pattern recognition*, pages 10684–10695, 2022.
- [51] Tim Salimans, Ian Goodfellow, Wojciech Zaremba, Vicki Cheung, Alec Radford, and Xi Chen. Improved techniques for training gans. *Advances in Neural Information Processing Systems*, 29, 2016.
- [52] Axel Sauer, Katja Schwarz, and Andreas Geiger. Stylegan-xl: Scaling stylegan to large diverse datasets. In *ACM SIGGRAPH 2022 conference proceedings*, pages 1–10, 2022.
- [53] Ying Shen, Yizhe Zhang, Shuangfei Zhai, Lifu Huang, Joshua M Susskind, and Jiatao Gu. Many-to-many image generation with auto-regressive diffusion models. *arXiv preprint arXiv:2404.03109*, 2024.
- [54] Ivan Skorokhodov, Sharath Girish, Benran Hu, Willi Menapace, Yanyu Li, Rameen Abdal, Sergey Tulyakov, and Aliaksandr Siarohin. Improving the diffusability of autoencoders. *arXiv preprint arXiv:2502.14831*, 2025.
- [55] Jianlin Su and Guang Wu. f-vaes: Improve vaes with conditional flows. *arXiv preprint arXiv:1809.05861*, 2018.
- [56] Peize Sun, Yi Jiang, Shoufa Chen, Shilong Zhang, Bingyue Peng, Ping Luo, and Zehuan Yuan. Autoregressive model beats diffusion: Llama for scalable image generation. *arXiv preprint arXiv:2406.06525*, 2024.
- [57] Yutao Sun, Hangbo Bao, Wenhui Wang, Zhiliang Peng, Li Dong, Shaohan Huang, Jianyong Wang, and Furu Wei. Multimodal latent language modeling with next-token diffusion. *arXiv preprint arXiv:2412.08635*, 2024.
- [58] NextStep Team, Chunrui Han, Guopeng Li, Jingwei Wu, Quan Sun, Yan Cai, Yuang Peng, Zheng Ge, Deyu Zhou, Haomiao Tang, et al. Nextstep-1: Toward autoregressive image generation with continuous tokens at scale. *arXiv preprint arXiv:2508.10711*, 2025.
- [59] Keyu Tian, Yi Jiang, Zehuan Yuan, Bingyue Peng, and Liwei Wang. Visual autoregressive modeling: Scalable image generation via next-scale prediction. *Advances in neural information processing systems*, 37:84839–84865, 2024.
- [60] Michael Tschannen, André Susano Pinto, and Alexander Kolesnikov. Jetformer: An autoregressive generative model of raw images and text. *arXiv preprint arXiv:2411.19722*, 2024.
- [61] Arash Vahdat, Karsten Kreis, and Jan Kautz. Score-based generative modeling in latent space. *Advances in neural information processing systems*, 34:11287–11302, 2021.
- [62] Aäron Van Den Oord, Nal Kalchbrenner, and Koray Kavukcuoglu. Pixel recurrent neural networks. In *International conference on machine learning*. PMLR, 2016.
- [63] Shuai Wang, Ziteng Gao, Chenhui Zhu, Weilin Huang, and Limin Wang. Pixnerd: Pixel neural field diffusion. *arXiv preprint arXiv:2507.23268*, 2025.

- [64] Shuai Wang, Zhi Tian, Weilin Huang, and Limin Wang. Decoupled diffusion transformer. [arXiv preprint arXiv:2504.05741](#), 2025.
- [65] Zhou Wang, Alan C Bovik, Hamid R Sheikh, and Eero P Simoncelli. Image quality assessment: from error visibility to structural similarity. [IEEE transactions on image processing](#), 13(4):600–612, 2004.
- [66] Jiawei Yang, Tianhong Li, Lijie Fan, Yonglong Tian, and Yue Wang. Latent denoising makes good visual tokenizers. [arXiv preprint arXiv:2507.15856](#), 2025.
- [67] Jingfeng Yao, Bin Yang, and Xinggong Wang. Reconstruction vs. generation: Taming optimization dilemma in latent diffusion models. In [Proceedings of the Computer Vision and Pattern Recognition Conference](#), pages 15703–15712, 2025.
- [68] Lijun Yu, José Lezama, Nitesh B Gundavarapu, Luca Versari, Kihyuk Sohn, David Minnen, Yong Cheng, Vighnesh Birodkar, Agrim Gupta, Xiuye Gu, et al. Language model beats diffusion–tokenizer is key to visual generation. [arXiv preprint arXiv:2310.05737](#), 2023.
- [69] Sihyun Yu, Sangkyung Kwak, Huiwon Jang, Jongheon Jeong, Jonathan Huang, Jinwoo Shin, and Saining Xie. Representation alignment for generation: Training diffusion transformers is easier than you think. [arXiv preprint arXiv:2410.06940](#), 2024.
- [70] Shuangfei Zhai, Ruixiang Zhang, Preetum Nakkiran, David Berthelot, Jiatao Gu, Huangjie Zheng, Tianrong Chen, Miguel Angel Bautista, Navdeep Jaitly, and Josh Susskind. Normalizing flows are capable generative models. [arXiv preprint arXiv:2412.06329](#), 2024.
- [71] Richard Zhang, Phillip Isola, Alexei A Efros, Eli Shechtman, and Oliver Wang. The unreasonable effectiveness of deep features as a perceptual metric. In [Proceedings of the IEEE conference on computer vision and pattern recognition](#), pages 586–595, 2018.
- [72] Ruixiang Zhang, Shuangfei Zhai, Jiatao Gu, Yizhe Zhang, Huangjie Zheng, Tianrong Chen, Miguel Angel Bautista, Josh Susskind, and Navdeep Jaitly. Flexible language modeling in continuous space with transformer-based autoregressive flows. [arXiv preprint arXiv:2507.00425](#), 2025.
- [73] Boyang Zheng, Nanye Ma, Shengbang Tong, and Saining Xie. Diffusion transformers with representation autoencoders. [arXiv preprint arXiv:2510.11690](#), 2025.
- [74] Guangting Zheng, Qinyu Zhao, Tao Yang, Fei Xiao, Zhijie Lin, Jie Wu, Jiajun Deng, Yanyong Zhang, and Rui Zhu. Farmer: Flow autoregressive transformer over pixels. [arXiv preprint arXiv:2510.23588](#), 2025.
- [75] Hongkai Zheng, Weili Nie, Arash Vahdat, and Anima Anandkumar. Fast training of diffusion models with masked transformers. [arXiv preprint arXiv:2306.09305](#), 2023.